Third-order correlation function and ghost imaging of chaotic thermal light in the photon counting regime

Yu Zhou, Jason Simon, Jianbin Liu, and Yanhua Shih
Department of Physics, University of Maryland, Baltimore County, Baltimore, MD 21250, USA
(Received 29 December 2009; published 26 April 2010)

In a near-field three-photon correlation measurement, we observed the third-order temporal and spatial correlation functions of chaotic thermal light in the single-photon counting regime. In the study, we found that the probability of jointly detecting three randomly radiated photons from a chaotic thermal source by three individual detectors is 6 times greater if the photodetection events fall in the coherence time and coherence area of the radiation field than if they do not. From the viewpoint of quantum mechanics, the observed phenomenon is the result of three-photon interference. By making use of this property, we measured the three-photon thermal light lensless ghost image of a double spot and achieved higher visibility compared with the two-photon thermal light ghost image.

DOI: 10.1103/PhysRevA.81.043831 PACS number(s): 42.50.Ar, 42.50.Dv, 03.65.Ud

I. INTRODUCTION

In 1995, Pittman *et al.* demonstrated the ghost-imaging phenomenon by using entangled photon pairs of spontaneous parametric down-conversion (SPDC) [1]. The important physics explored in the ghost-imaging experiment is the nonlocal, point-to-point correlation in the joint detection of the entangled signal-idler photon pair:

$$g^{(2)}(\vec{\rho}_o, \vec{\rho}_i) \sim \delta(\vec{\rho}_o + \vec{\rho}_i/m), \tag{1}$$

where $g^{(2)}(\vec{\rho}_o, \vec{\rho}_i)$ is the normalized second-order correlation function; $\vec{\rho}_o$ and $\vec{\rho}_i$ are the transverse coordinates on the object plane and the image plane, respectively; and m is the magnification factor of the image. The observed ghost image in the integrated coincidences is the result of a convolution between the aperture function and the nonfactorizable, point-to-point image-forming correlation function. In the language of Einstein-Podolsky-Rosen (EPR), in this measurement, neither the signal photon nor the idler photon knows where to go in the course of its propagation (nondeterministic); however, if the signal is observed at a certain point on the image plane, the idler must be measured at a unique point on the object plane simultaneously, despite the distance between them.

Ten years after the ghost-imaging experiment of Pittman *et al.*, Valencia *et al.* found that the natural, nonfactorizable, point-to-point image-forming correlation is not only the property of entangled photon pairs [2,3]. It can be realized in the joint detection of an arbitrary pair of randomly distributed photons of chaotic thermal radiation in a lensless near-field configuration, except with a 50% constant background noise:

$$g^{(2)}(\vec{\rho}_o, \vec{\rho}_i) \sim 1 + \delta(\vec{\rho}_o - \vec{\rho}_i). \tag{2}$$

The jointly measured photon pair in thermal light ghost imaging are just two independent, randomly distributed photons that fall into the coincidence time window only by chance. To obtain an observable ghost image with recognizable visibility, the natural, nonfactorizable, point-to-point image-forming correlation of thermal light must be observable at the quantum level. In the language of EPR, in this measurement, neither photon 1 nor photon 2 knows where to go in the course of its propagation (nondeterministic); however, if photon 1 is observed at a certain point on the image plane, photon 2 has twice the probability of being measured at a unique point on the object plane simultaneously, despite the distance between them.

The point-to-point image-forming correlation of ghost imaging can be simulated classically to reproduce ghost images in a deterministic manner [4]. There have been several classical approaches to simulate the point-to-point ghost image-forming correlation. Bennink *et al.* [5] and Gatti *et al.* [6] suggested two types of classical simulations to reproduce ghost-imaging effects. One uses correlated laser beams, and the other uses two sets of correlated identical classical images of "speckles" of the light source. Different from the randomly distributed and propagated chaotic light or entangled photon pairs in ghost imaging, in these classical simulations, the light knows "where to go" during the course of its propagation: The radiations are prepared in such a way that each light beam or intensity "speckle" is propagated to a precise chosen "spot" of the object. For each detection, the coordinate on the object $\vec{\rho_{\rm obj}}$, which is chosen by the light source, is recorded against the counting rate of the bucket detector at that coordinate, which is proportional to the aperture function $|A(\vec{\rho_{\rm obj}})|^2$. The aperture function $A(\vec{\rho_{\rm obj}})$ is thus calculated after a large number of such records.

One of the disadvantages of second-order thermal light ghost imaging compared with ghost imaging of entangled photon pairs is the low image contrast, which is always below 50%. On the other hand, the contrast of entangled photon ghost imaging can achieve 100% under the condition of "no more than one coincidence event" within the coincidence time window. It is the contrast that distinguishes classical from quantum correlation like ghost imaging, ghost interference, where quantum schemes usually give very high contrast but at low counting rates [5,7–9]. In this article, we will find that measuring the third-order instead of the second-order correlation function may help to boost the contrast in classical schemes. The more appealing aspect is that in theory, by measuring the Nth-order correlation, we could expect the contrast to achieve 100% using a thermal light source [10].

It is also the aim of this article to provide a basic picture and understanding of the higher order correlation of thermal light in the photon-counting regime. In this article, we report the direct

measurement of the temporal and spatial distributions of the third-order correlation function of pseudothermal light using single photon detectors. One important difference between this article and other publications on high-order correlation function measurements [11] is that we directly measure the third-order correlation function of thermal light in the photon-counting regime. In this article, we also report the third-order thermal light lensless ghost imaging by making use of this property. In the measurement, the visibility of ghost imaging was significantly improved compared to second-order ghost imaging.

The article is organized as follows. First we will introduce the quantum theory about the third-order correlation function of thermal light in Sec. II. In Sec. III and Sec. IV, we report the measurement of the third-order temporal and spatial correlation functions of pseudothermal light, respectively. In Sec. V, we present the third-order lensless thermal light ghost imaging and the comparison between it and the second-order ghost imaging. The conclusion is in Sec. VI.

II. THEORY

In classical theory, the far-field Hanbury Brown and Twiss effect (HBT) is interpreted as the result of intensity fluctuation correlation: When the two detectors D_1 and D_2 measure the same mode of the radiation field, the intensities they measure have the same fluctuation, and $\langle \Delta I_1 \Delta I_2 \rangle$ has a maximum value. However, in the photon-counting regime where the light is so weak that only a few photons are in the field, we can still find the photons arriving in a correlated way by photon counting. Classical theory faces difficulty because there is no "intensity fluctuation" there. This is not a trivial phenomenon given that the chaotic source emits photons randomly and the quantum mechanical interpretation is more reasonable. From the quantum mechanical point of view, the HBT effect comes from the coherent superposition of two probability amplitudes, nonclassical entities corresponding to different yet indistinguishable alternative ways of triggering a two-photon joint-detection event [3,12].

In a similar way, the third-order correlation of thermal light comes from a coherent superposition of six different yet indistinguishable probability amplitudes, as shown in Fig. 1. There are three independent photons a, b, and c and three detectors D_1, D_2, and D_3. There are six different ways for the three photons to trigger the three detectors. For example, in the first case, photon a triggers detector D_1, photon b triggers detector D_2, and photon c triggers detector D_3. This is one of the ways to trigger a three-photon joint-detection event, named as probability amplitude A_I. The definitions of other probability amplitudes are similar.

The probability of a three-photon joint detection event happening is the modulus square of the sum of all six probability amplitudes:

$$P_{3CC} = |A_{\mathrm{I}} + A_{\mathrm{II}} + A_{\mathrm{III}} + A_{\mathrm{IV}} + A_{\mathrm{V}} + A_{\mathrm{VI}}|^2. \quad (3)$$

When the six probability amplitudes superpose coherently, the probability of having a triple coincidence count achieves a maximum with the contribution from the cross-terms in Eq. (3). The prerequisite of the coherent superposition of the six different probability amplitudes is that the amplitudes

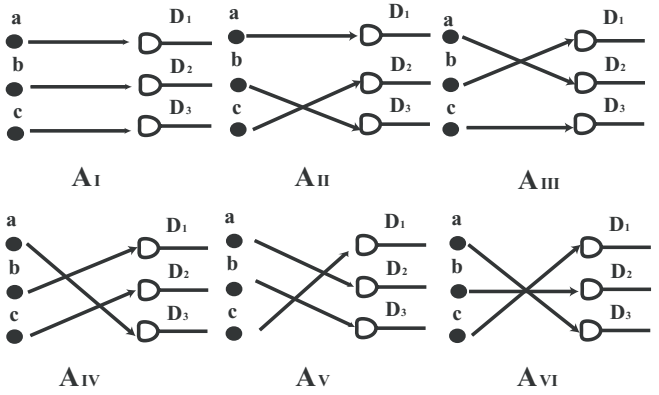

FIG. 1. Three independent photons a, b, and c have six alternative ways of triggering a joint-detection event between detectors D_1, D_2, and D_3. At equal distances from the source, the probability of observing a three-photon joint-detection event at space-time $(\mathbf{r}_1,\mathbf{r}_2,\mathbf{r}_3)$ is determined by the superposition of the six three-photon amplitudes. At $\mathbf{r}_1 = \mathbf{r}_2 = \mathbf{r}_3$, six amplitudes superpose constructively. $G^{(3)}(\mathbf{r}_1,\mathbf{r}_2,\mathbf{r}_3)$ achieves its maximum value because of constructive interferences.

have the same phase or, equivalently, the three photons have momenta and positions belonging to the same elementary cell in phase space [13,14]. In this case, all three photons in the same cell are *in principle* indistinguishable from one another. To describe the triple joint detection event triggered by the three identical and indistinguishable photons which are bosons, the effective wave function must have a symmetric form. This is the key to understanding the quantum interference of three-photon amplitudes: The symmetrized effective wave function, which is equivalent to the coherent superposition of probability amplitudes, leads to the constructive interference. The constructive interference leads to the cross-terms in Eq. (3) being not zero, so there are 36 terms altogether.

On the other hand, if the three photons are from different elementary cells in phase space, the six probability amplitudes in Fig. 1, which are in principle distinguishable from each other, do not superpose coherently. The cross-terms in Eq. (3) are equal to zero, and the probability of triple coincidence counts reduces to

$$P_{3CC} = |A_{\mathrm{I}}|^2 + |A_{\mathrm{II}}|^2 + |A_{\mathrm{III}}|^2 + |A_{\mathrm{IV}}|^2 + |A_{\mathrm{V}}|^2 + |A_{\mathrm{VI}}|^2. \quad (4)$$

We notice that in Eq. (3), there are 36 terms, and there are only 6 terms in Eq. (4), so the ratio is 6 to 1: When the three photons are from the same elementary cell in phase space, the probability of having a triple coincident count is 6 times greater than when the three photons are from different elementary cells in phase space.

In the preceding, we have the intuitive description of the third-order correlation function of thermal light. To calculate it in detail, we need to start from Glauber's definition of the correlation function [15]:

$$G^{(3)}(\mathbf{r}_1,\mathbf{r}_2,\mathbf{r}_3) = \langle \hat{E}_1^{(-)}(\mathbf{r}_1)\hat{E}_2^{(-)}(\mathbf{r}_2)\hat{E}_3^{(-)}(\mathbf{r}_3)\hat{E}_3^{(+)}(\mathbf{r}_3)\hat{E}_2^{(+)}(\mathbf{r}_2)\hat{E}_1^{(+)}(\mathbf{r}_1)\rangle, \quad (5)$$

where $\langle\cdots\rangle$ denotes an expectation value operation based on the quantum state of the measured electromagnetic field and $\mathbf{r}_1$, $\mathbf{r}_2$, and $\mathbf{r}_3$ stand for different space times that detectors are triggered. Thermal radiation is in mixed states. The generalized density operator for a chaotic thermal field can be written as [14]

$$\hat{\rho} = \sum_{\{n\}} p_{\{n\}} |\{n\}\rangle\langle\{n\}|, \tag{6}$$

where $p_{\{n\}}$ is the probability that the thermal field is in the state

$$|\{n\}\rangle \equiv \prod_{\mathbf{k}} |n_{\mathbf{k}}\rangle = |n_{\mathbf{k}}\rangle|n_{\mathbf{k}'}\rangle\cdots|n_{\mathbf{k}''\cdots'}\rangle.$$

where $\mathbf{k}$ is the wave vector. The summation of Eq. (6) includes all possible modes $\mathbf{k}$, all possible occupation numbers $n_{\mathbf{k}}$ for the mode $\mathbf{k}$, and all possible combinations of occupation numbers for different modes in a set of $\{n\}$. In the following, we will calculate the third-order temporal and spatial correlation function of thermal light.

A. The third-order temporal correlation function

To calculate the third-order temporal correlation function, we assume that the three detectors are placed in the same coherent area and fixed in the transverse plane. Furthermore, we simplify the problem to 1-D (temporal) with one polarization. In this case, the density matrix to describe the thermal radiation is

$$\hat{\rho}_{a,b,c} = \sum_{a,b,c} P_{a,b,c} |\psi_{a,b,c}\rangle\langle\psi_{a,b,c}|, \tag{7}$$

where $P_{a,b,c}$ is the probability of finding the radiation in the state $|\psi_{a,b,c}\rangle$ and will be assumed constant in the following. The state $|\psi_{a,b,c}\rangle$ is the tensor product of three independent multimode single photon states [16]:

$$\begin{aligned}|\psi_{a,b,c}\rangle &= |\psi_a\rangle|\psi_b\rangle|\psi_c\rangle \\ &= \int d\omega_a f(\omega_a) e^{-i\omega_a t_{0a}} a^\dagger(\omega_a)|0\rangle \\ &\quad\times \int d\omega_b f(\omega_b) e^{-i\omega_b t_{0b}} a^\dagger(\omega_b)|0\rangle \\ &\quad\times \int d\omega_c f(\omega_c) e^{-i\omega_c t_{0c}} a^\dagger(\omega_c)|0\rangle,\end{aligned} \tag{8}$$

where the $f(\omega)$ is the spectral distribution function and t_{0a}, t_{0b}, and t_{0c} are the creation times of the individual photons, respectively.

In Eq. (5), the quantized field operators take the following form:

$$\hat{E}_j^{(-)}(t_j) = \int d\omega_j\, g(\omega_j,t_j)\, \hat{a}^\dagger(\omega_j) \quad (j = 1,2,3), \tag{9}$$

where $g(\omega_j,t_j)$ is the Green's function which propagates each longitudinal mode ω_j of the field from the source to the jth detector in the longitudinal direction and t_1, t_2, and t_3 stand for the times when detectors D_1, D_2, and D_3 are triggered, respectively.

Combining Eq. (5), Eq. (7), and Eq. (9), and assuming that the thermal field contains very few photons (our experiments are done in a photon-counting regime), Eq. (5) can be written as

$$\begin{aligned}G^{(3)}(t_1,t_2,t_3) &= \mathrm{Tr}\{\hat{\rho}_{a,b,c}\hat{E}_1^{(-)}(t_1)\hat{E}_2^{(-)}(t_2)\hat{E}_3^{(-)}(t_3) \\ &\quad\times \hat{E}_3^{(+)}(t_3)\hat{E}_2^{(+)}(t_2)\hat{E}_1^{(+)}(t_1)\} \\ &= \sum_{a,b,c} P_{a,b,c}|\langle 0|\hat{E}_3^{(+)}(t_3)\hat{E}_2^{(+)}(t_2)\hat{E}_1^{(+)}(t_1)|\psi_{a,b,c}\rangle|^2,\end{aligned} \tag{10}$$

where $\langle 0|\hat{E}_3^{(+)}(t_3)\hat{E}_2^{(+)}(t_2)\hat{E}_1^{(+)}(t_1)|\psi_{a,b,c}\rangle$ is defined as a three-photon detection effective wave function.

Substituting Eq. (8) and Eq. (9) into Eq. (10), for continuous and random distribution of t_{0a}, t_{0b}, and t_{0c}, after the ensemble average, the third-order temporal correlation function of thermal light is [10]

$$\begin{aligned}G^{(3)}(t_1,t_2,t_3) \propto \int d\omega_a\, d\omega_b\, d\omega_c |f(\omega_a)|^2|f(\omega_b)|^2|f(\omega_c)|^2 \\ \times\Big|\frac{1}{\sqrt{6}}[g(\omega_a,t_1)g(\omega_b,t_2)g(\omega_c,t_3) \\ + g(\omega_a,t_1)g(\omega_c,t_2)g(\omega_b,t_3) \\ + g(\omega_b,t_1)g(\omega_a,t_2)g(\omega_c,t_3) \\ + g(\omega_b,t_1)g(\omega_c,t_2)g(\omega_a,t_3) \\ + g(\omega_c,t_1)g(\omega_a,t_2)g(\omega_b,t_3) \\ + g(\omega_c,t_1)g(\omega_b,t_2)g(\omega_a,t_3)]\Big|^2,\end{aligned} \tag{11}$$

where $g(\omega_k,t_j) \propto e^{-i\omega_k t_j}$ $(k = a,b,c;\, j = 1,2,3)$ is the Green's function which propagates mode ω_k of photon k to detector j (assuming that the three detectors are in the same coherence area). Equation (11) is the key equation to understanding the three-photon interference nature of the third-order correlation. The six effective wave functions in Eq. (11) correspond to six different alternative ways for three independent photons to trigger a threefold joint-detection event (see Fig. 1). Since the three detectors are at an equal distance from the source, the six amplitudes superpose constructively at $t_1 = t_2 = t_3$, and consequently, $G^{(3)}(t_1,t_2,t_3)$ achieves its maximum value.

On the other hand, when $t_1 \neq t_2 \neq t_3$ and the difference is bigger than the coherence time of light field [as shown in Eq. (13)], the cross-terms equal zero, and consequently, $G^{(3)}(t_1,t_2,t_3)$ reduces to

$$\begin{aligned}G^{(3)}(t_1,t_2,t_3) \propto \int d\omega_a\, d\omega_b\, d\omega_c |f(\omega_a)|^2|f(\omega_b)|^2|f(\omega_c)|^2 \\ \times\frac{1}{6}[|g(\omega_a,t_1)g(\omega_b,t_2)g(\omega_c,t_3)|^2 \\ + |g(\omega_a,t_1)g(\omega_c,t_2)g(\omega_b,t_3)|^2 \\ + |g(\omega_b,t_1)g(\omega_a,t_2)g(\omega_c,t_3)|^2 \\ + |g(\omega_b,t_1)g(\omega_c,t_2)g(\omega_a,t_3)|^2 \\ + |g(\omega_c,t_1)g(\omega_a,t_2)g(\omega_b,t_3)|^2 \\ + |g(\omega_c,t_1)g(\omega_b,t_2)g(\omega_a,t_3)|^2].\end{aligned} \tag{12}$$

Comparing Eq. (11) with Eq. (12), we know that from the quantum mechanical point of view, it is the three-photon interference that causes the three randomly distributed photons

to have 6 times more chance of being detected at $t_1 = t_2 = t_3$ than at $t_1 \neq t_2 \neq t_3$.

To evaluate Eq. (11), we simplify the calculation by taking the spectral function $f(\omega)$ as a constant within the narrow bandwidth $\Delta\omega$ of the thermal light field; the normalized third-order correlation function $g^{(3)}(t_1,t_2,t_3)$ is

$$g^{(3)}(t_1,t_2,t_3) = 1 + \mathrm{sinc}^2\left[\frac{\Delta\omega(t_1-t_2)}{2}\right] + \mathrm{sinc}^2\left[\frac{\Delta\omega(t_2-t_3)}{2}\right] + \mathrm{sinc}^2\left[\frac{\Delta\omega(t_3-t_1)}{2}\right] + 2\,\mathrm{sinc}\left[\frac{\Delta\omega(t_1-t_2)}{2}\right] \times \mathrm{sinc}\left[\frac{\Delta\omega(t_2-t_3)}{2}\right]\mathrm{sinc}\left[\frac{\Delta\omega(t_3-t_1)}{2}\right]. \quad (13)$$

From Eq. (13), we can see that when $t_1 = t_2 = t_3$, $g^{(3)}(t_1,t_2,t_3) = 6$, the third-order correlation function achieves a maximum contrast of 6 to 1 (visibility ~71%). Phenomenologically, we may name the three-photon correlation "three-photon bunching." From the quantum mechanical point of view, this bunching is the result of three-photon interference, the coherent superposition of three-photon probability amplitudes.

B. The third-order spatial correlation function

The calculation of the third-order spatial correlation function is similar to that of the temporal correlation function. To simplify the calculation, we assume that the thermal light source is quasimonochromatic and that the three detectors are placed the same distance from the light source in the longitudinal direction; also, the light has a single polarization mode. Furthermore, we assume that the three detectors have the same y coordinate values in the transverse plane to simplify the problem to 1-D. The density matrix to describe the thermal field is

$$\hat{\rho}_{a,b,c} = \sum_{a,b,c} P_{a,b,c}|1_{q_a}1_{q_b}1_{q_c}\rangle\langle 1_{q_a}1_{q_b}1_{q_c}|, \quad (14)$$

where $P_{a,b,c}$ is the probability of finding the radiation in the state $|1_{q_a}1_{q_b}1_{q_c}\rangle$ and will be assumed constant in the following: q_a, q_b, and q_c stand for transverse wave vectors in the x direction for photons a, b, and c, respectively.

The quantized field operators take the following form:

$$\hat{E}_j^{(-)}(x_j) = \int dk_x\, g(k_x,x_j)\,\hat{a}^\dagger(k_x) \quad (j = 1,2,3), \quad (15)$$

where $g(k_x, x_j)$ is the Green's function which propagates the transverse mode k_x from the source to the jth detector. The x_j is the coordinate of the jth detector. The calculation of Green's function can be found in Refs. [10,17]:

$$g(k_x,x_j) \propto -i\frac{\omega}{2\pi c}\frac{e^{i\frac{\omega}{c}z}}{z}\int dx_s \psi\left(|x_s - x_j|, \frac{\omega}{cz}\right)e^{ik_x x_s}, \quad (16)$$

where $\psi(|x_s - x_j|, \omega/cz) = e^{i(\omega/2cz)|x_s - x_j|^2}$, z is the distance between the source and the detectors, and x_s is the coordinate on the source plane.

The following calculation is similar to that shown in Eq. (10) and Eq. (11). Finally, the normalized third-order spatial correlation function of thermal light is [10]

$$g^{(3)}(x_1,x_2,x_3) = 1 + \mathrm{sinc}^2\left[\frac{\pi\Delta\theta}{\lambda}(x_1-x_2)\right] + \mathrm{sinc}^2\left[\frac{\pi\Delta\theta}{\lambda}(x_2-x_3)\right] + \mathrm{sinc}^2\left[\frac{\pi\Delta\theta}{\lambda}(x_3-x_1)\right] + 2\mathrm{sinc}\left[\frac{\pi\Delta\theta}{\lambda}(x_1-x_2)\right] \times \mathrm{sinc}\left[\frac{\pi\Delta\theta}{\lambda}(x_2-x_3)\right]\mathrm{sinc}\left[\frac{\pi\Delta\theta}{\lambda}(x_3-x_1)\right], \quad (17)$$

where x_1, x_2, and x_3 are the transverse positions of detectors D_1, D_2, and D_3, respectively; $\Delta\theta$ is the angular size of the source viewed from the detectors. From Eq. (17), we can see that when $x_1 = x_2 = x_3$, the six amplitudes superpose coherently, and $g^{(3)}(x_1, x_2, x_3)$ achieves its maximum value of 6. On the other hand, when $x_1 \neq x_2 \neq x_3$ and the differences are bigger than the transverse coherence length $\lambda/\Delta\theta$, the six amplitudes do not superpose coherently, the cross-terms become equal to zero, and $g^{(3)}(x_1, x_2, x_3)$ achieves the lowest value of 1. From the quantum mechanical point of view, it is the interference of three-photon probability amplitudes that causes the three randomly distributed photons to have 6 times more chance of being captured at $x_1 = x_2 = x_3$ than of being captured at $x_1 \neq x_2 \neq x_3$, where the distances between detectors are bigger than the transverse coherence lengths in the x direction.

III. MEASURING THE THIRD-ORDER TEMPORAL CORRELATION FUNCTION OF PSEUDOTHERMAL LIGHT

The experimental setup for measuring the third-order temporal correlation function of pseudothermal light is shown schematically in Fig. 2. The light source is a standard pseudothermal source which contains a cw laser beam, a fast-rotating diffusing ground glass, and a focal lens (with a 25.4-mm focal length). The 632.8-nm laser beam is focused by the lens onto the rotating ground glass. The diameter of the light spot on the glass is less than 100 μm. The coherent laser beam is scattered by the fast-rotating ground glass to simulate a thermal field with ~0.2-μs coherence time. The coherence time of pseudothermal light is determined by the angular speed of the disk, the curvature of the focused laser beam, and the transverse distance between the pinhole and the laser beam; the detailed

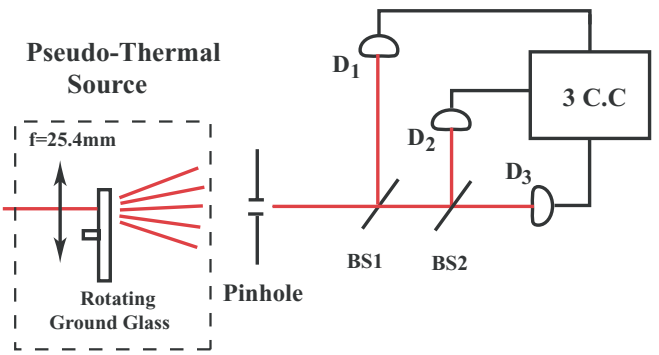

FIG. 2. (Color online) Schematic for measuring the third-order temporal correlation function of pseudothermal light.

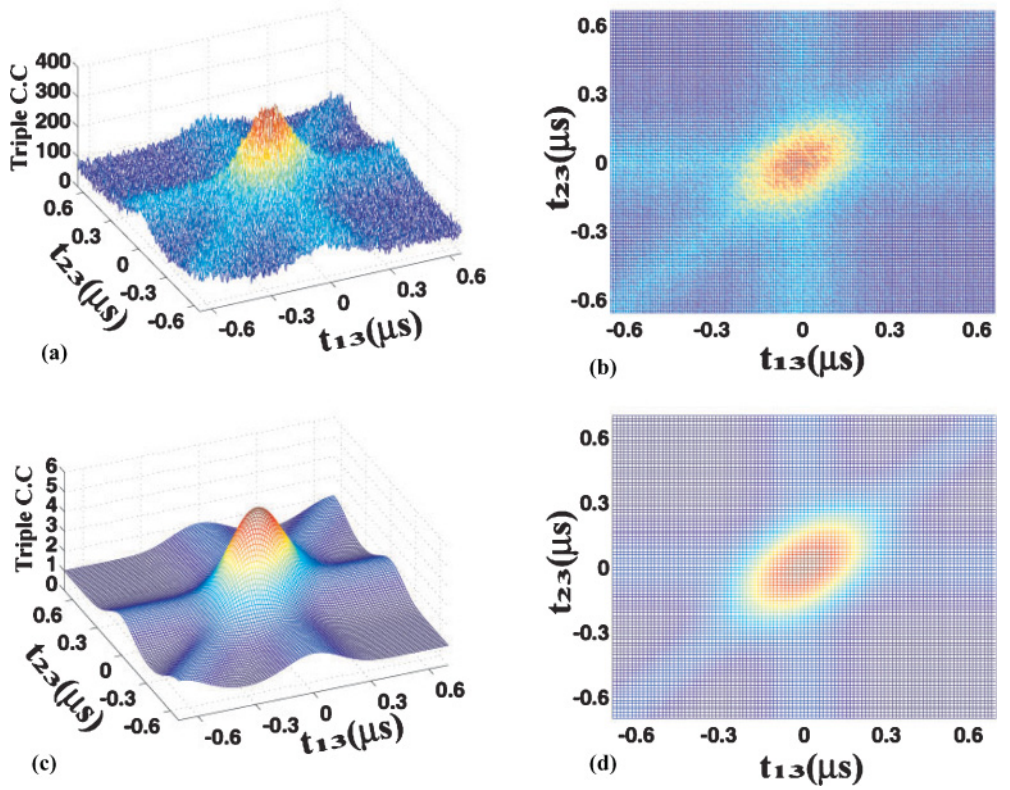

FIG. 3. (Color online) (a, b) Measured and (c, d) calculated third-order temporal correlation function of thermal light. The 3-D three-photon joint detection histogram is plotted as a function of $t_{13} \equiv t_1 - t_3$ and $t_{23} \equiv t_2 - t_3$. The simulation function is calculated from Eq. (13).

discussion can be found in Ref. [18]. Effectively, the rotating ground glass produces a large number of independent point subsources (3–5 μm in diameter) with independent random phases. A pinhole with a diameter size $\sim$1 mm is placed 800 mm away from the ground glass to select a small portion of the radiation within its spatial coherence area. At this distance, the size of the coherent area is $\sim$10 mm. The pseudothermal light passes through beam splitters BS1 and BS2. The transmitted radiation is detected by photon detector D_3, and the reflected radiations are detected by photon detectors D_1 and D_2. To simplify the discussion, we achieved equal intensities in the three paths by manipulating the transmission-reflection coefficients of the two beam splitters and had equal distances between the light source and the three photon detectors. D_1, D_2, and D_3 are fast avalanche photodiodes working in the photon-counting regime. The photo-detection response time is on the order of a few hundred picoseconds, which is much shorter than the $\sim$0.2-μs coherence time of the radiation. The output pulses from D_1, D_2, and D_3 are sent to a threefold coincidence counting circuit which provides a three-photon counting histogram as a function of $t_2 - t_3$ and $t_1 - t_3$, where $t_j, j = 1,2,3$, is the registration time of the photodetection event at D_1, D_2, and D_3, respectively. In addition, the single-detector counting rates for D_1, D_2, and D_3 are all monitored to be constant during the measurement.

The experimentally measured and simulated 3-D third-order temporal correlation functions are reported in the upper and lower parts of Fig. 3, respectively. The simulation is calculated based on Eq. (13). It is easy to see that (1) the randomly radiated photons have 6 times greater chance of being jointly detected in triples when $t_1 = t_2 = t_3$ than when $t_1 \neq t_2 \neq t_3$ and (2) the measured correlation function is close to the simulation.

From Eq. (13), we know that in order to claim that the measured correlation is the third-order effect, the contrast between the peak and the background should be larger than 4 to 1, corresponding to a visibility larger than 60%. To compare the joint counting rate at $t_1 = t_2 = t_3$ with the joint counting rate at $t_1 \neq t_2 \neq t_3$, a sliced cross section of the measured 3-D histogram is illustrated in Fig. 4. The plot is a 2-D cross

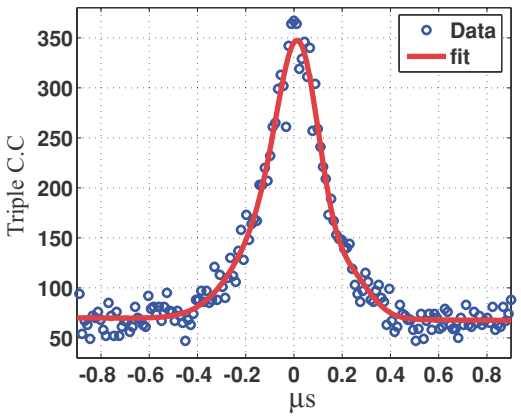

FIG. 4. (Color online) Cross section of the three-photon coincidence counting histogram, which is sliced from the top left corner to the bottom right corner of Fig. 3(b). The contrast between the maximum counting rate and the constant background is 4.9 ± 0.25 to 1, indicating a nontrivial third-order correlation with visibility of $\sim$66%.

section of Fig. 3(b) sliced from the top left corner to the bottom right corner. The contrast between the maximum counting rate, which occurs at $t_1 = t_2 = t_3$, and the constant background is 4.9 ± 0.25 to 1, indicating the third-order correlation function with visibility of ~66%, which is greater than the 2 to 1 contrast (33% visibility) of HBT. This result shows that thermal light has a much greater chance of bunching in triples rather than in pairs. The theoretically expected contrast is 6 to 1 (71% visibility). We think the reason for observing a lower visibility than the theoretical prediction may be the finite size of the detector. We hope to achieve higher visibility by simulating ideal point detectors.

IV. MEASURING THE THIRD-ORDER SPATIAL CORRELATION FUNCTION OF PSEUDOTHERMAL LIGHT

The experimental scheme for measuring the third-order spatial correlation function of pseudothermal light is given in Fig. 5. The pseudothermal source comprises a He-Ne laser, a focal lens with 25.4 mm focus length, and a rotating ground glass. The diameter of the focused spot on the ground glass is about 2 mm. The pseudothermal beam is divided into three by two beam splitters BS1 and BS2. We simulate three point detectors D_1, D_2, and D_3 using three avalanche single photon detectors with fiber tips (the diameter of the fiber tips is about 6 μm). To simplify the discussion, we achieved equal intensities in the three paths by manipulating the transmission-reflection coefficients of the two beam splitters and had equal distances (~870 mm) between the light source and the three photon detectors. The spatial correlation function is measured in the near-field of thermal light ($\Delta\theta \sim 7\lambda/d$).

The third-order spatial correlation function of thermal light described in Eq. (17) is the function of variables $x_1 - x_2$, $x_2 - x_3$, and $x_3 - x_1$, where x_1, x_2, and x_3 stand for the transverse positions in the x direction of detectors D_1, D_2, and D_3, respectively. (Because the three variables are not independent, only two are enough to describe the correlation function.) To measure it in our experiment, we keep the detector D_1 always fixed and move detectors D_2 and D_3 to sample the correlation function. If both detectors D_1 and D_2 are fixed at position zero, that is, $x_1 = x_2 = 0$, and we scan the detector D_3 to record the triple coincidence counts, that is equivalent to sampling the correlation function along line I in the x_{13} and x_{23} planes, as shown in Fig. 6. (The x_{13} stands for the variable $x_1 - x_3$ and x_{23} stands for variable $x_2 - x_3$, respectively.) If we keep detector D_1 at position zero ($x_1 = 0$)

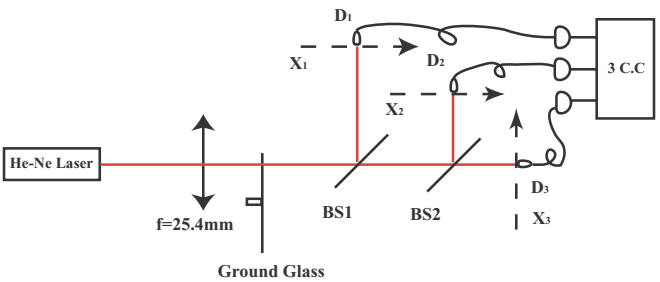

FIG. 5. (Color online) Schematic for measuring the third-order spatial correlation function of pseudothermal light.

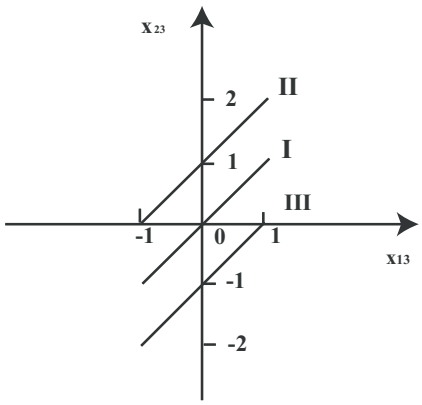

FIG. 6. To measure the third-order spatial correlation function of pseudothermal light, which is a function of the variables $x_1 - x_2$, $x_2 - x_3$, and $x_3 - x_1$ (x_1, x_2, and x_3 stand for the transverse positions of detector D_1, D_2, and D_3, respectively), we keep the detector D_1 always fixed and move detectors D_2 and D_3 to sample the spatial correlation function. For example, both detectors D_1 and D_2 are fixed at position zero, i.e., $x_1 = x_2 = 0$, and we scan the detector D_3 to record the triple coincidence counts, which is equivalent to sampling the correlation function along line I in the x_{13} and x_{23} planes. If we keep detector D_1 at position zero ($x_1 = 0$), if we keep detector D_2 at position 1 ($x_2 = 1$), and if we scan the detector $D3$ to record the triple coincidence counts, that is equivalent to sampling the correlation function along line II in the x_{13} and x_{23} planes. If we keep detector D_1 at position zero ($x_1 = 0$), if we keep detector D_2 at position -1 ($x_2 = -1$), and if we scan the detector D_3 to record the triple coincidence counts, that is equivalent to sampling the correlation function along line III in the x_{13} and x_{23} planes. In the scanning, the single counting rate of detector D_3 is constant.

and detector D_2 at position 1 ($x_2 = 1$) and we scan the detector D_3 to record the triple coincidence counts, that is equivalent to sampling the correlation function along line II in Fig. 6. If we keep detector D_1 at position zero ($x_1 = 0$) and detector D_2 at position -1 ($x_2 = -1$) and we scan the detector D_3 to record the triple coincidence counts, that is equivalent to sampling the correlation function along line III in Fig. 6. By so doing, we measure the spatial distribution of the third-order correlation function.

The measured and simulated third-order spatial correlation functions of pseudothermal light are shown in Fig. 7 (top) and Fig. 7 (bottom), respectively. The simulated result is based on Eq. (17). The contrast of the measured third-order correlation function is about 4.8 ± 0.2 to 1. In order to get enough triple coincidences in the measurement, we need the coincidence window to be big, which may decrease the visibility of the correlation function.

Although the measured contrast is not as high as the theoretical prediction (6 to 1), it is still higher than that of the second-order correlation (2 to 1). More interesting, the contrast of the Nth-order correlation function of thermal light can be $N!$ to 1 [10], which means that one can expect higher contrast of the image in third-order or higher thermal light ghost imaging. This is appealing since thermal light ghost imaging may have important applications in the future [19]. In the next section, we present the thermal light three-photon lensless ghost-imaging experiment in the single photon-counting regime.

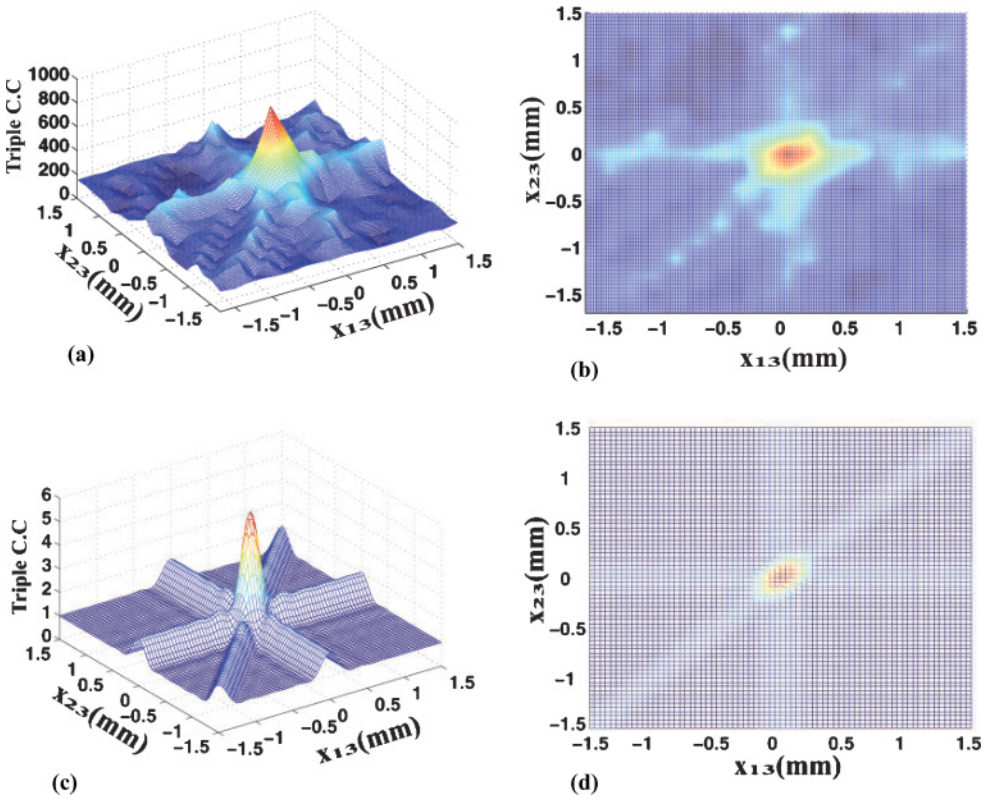

FIG. 7. (Color online) (a, b) Measured and (c, d) calculated third-order spatial correlation function of thermal light. The 3-D three-photon joint detection histogram is plotted as a function of $x_{13} \equiv x_1 - x_3$ and $x_{23} \equiv x_2 - x_3$. The simulation function is calculated from Eq. (17). In addition, the single-detector counting rates for D_1, D_2, and D_3 are monitored to be constant in measurement.

V. MEASURING THE THREE-PHOTON THERMAL LIGHT LENSLESS GHOST IMAGE OF A DOUBLE SPOT

The experimental scheme of the three-photon thermal light lensless ghost-imaging setup is shown in Fig. 8. The pseudothermal light source is composed of a He-Ne laser, a focal lens (with 25.4 mm focal length), and a rotating diffusing ground glass. The laser beam is focused onto the ground glass with ∼1 mm diameter by the focal lens. The ground glass scatters the focused laser beam and introduces extremely complex and irregular distortion to the incident wavefront, which creates pseudothermal light. The pseudothermal light passes through the beam splitter and splits into two beams. The reflected beam, usually called the "object beam," is coupled into a 2×1 fiber coupler and input to the single photon detector D_1. The fiber tip t_1 is about 0.7 mm left of center, and the fiber tip t_2 is about 0.7 mm right of center of the reflected beams. Effectively, the 2×1 fiber coupler and detector D_1 function as a bucket detector, and the two fiber tips function as a double spot. The transmitted beam, usually called the "reference beam," is collected by the fiber tip t_3 on the plane X_2 and then splits into two beams in the 1×2 fiber splitter and is sent to single photon detectors D_2 and D_3. The distance between the ground glass and the planes X_1 and X_2 is 870 mm. To simplify the discussion, we achieve equal single-counting rates for all the detectors. In the measurement, the fiber tips t_1 and t_2 are fixed in the plane X_1, and we scan the fiber tip t_3 in the plane X_2. The output of the detectors is input into the triple coincidence circuit. To compare the three-photon lensless ghost imaging with the two-photon lensless ghost imaging, we just need to turn of detector D_2 and measure the coincidence counts between detectors D_1 and D_3 during scanning.

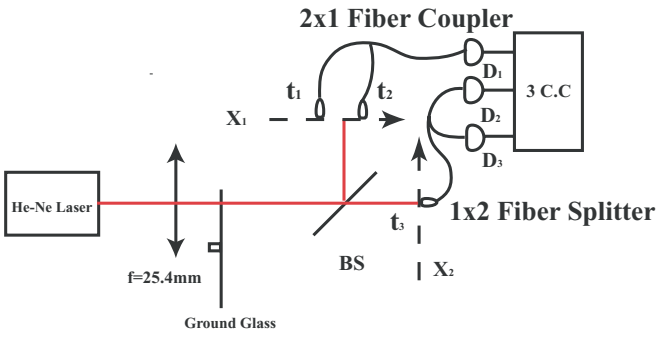

FIG. 8. (Color online) A 2×1 fiber coupler is used to simulate the double spot. Fiber tip t_1 on plane X_1 is about 0.7 mm left of center, and fiber tip 2 is about 0.7 mm right of center of the reflected beams. Effectively, the fiber coupler and detector D_1 function as a bucket detector, and the two fiber tips function as a double spot. The transmitted beam is collected by fiber tip 3 on plane X_2 and then is split into two beams in the 1×2 fiber splitter and sent to single photon detector D_2 and D_3. In the experiment, we scan fiber tip 3 on plane X_2 and record the triple coincidence counts to measure the three-photon ghost image. We can also measure the two-photon ghost image by turning off detector D_2 and recording the joint coincidence counts between detectors D_1 and D_3 during scanning.

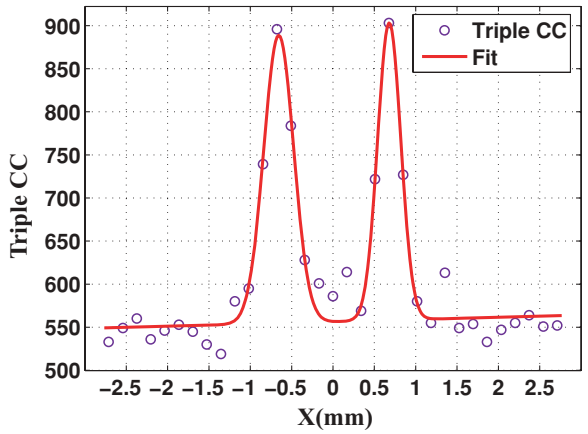

FIG. 9. (Color online) The three-photon lensless ghost image of a double spot. The y axis stands for triple coincidence counts collected in 180 s, and the x axis stands for the coordinates of the fiber tip on the X_2 plane. The single counting rates of detectors D_2 and D_3 are constant during scanning. The visibility of the three-photon lensless ghost image is ∼25%.

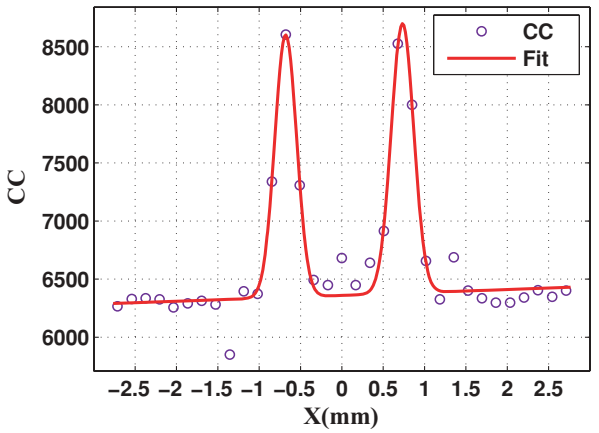

FIG. 10. (Color online) The two-photon lensless ghost image of double spots. The y axis stands for joint coincidence counts collected in 10 s, and the x axis stands for the coordinates of the fiber tip on the X_2 plane. The single counting rate of detector D_3 is constant when we scan fiber tip t_3. The visibility of the two-photon lensless ghost image is ∼12%.

The measurement result of the three-photon lensless ghost imaging is shown in Fig. 9. In Fig. 9, the y axis stands for triple coincidence counts collected in 180 s, and the x axis stands for the coordinate of the fiber tip on the detection plane X_2. The circles in the figure stand for the data and the solid line is the fit curve. In the measurement, the single-counting rates of detectors D_2 and D_3 are monitored as constant when fiber tip t_3 scans. The data show that the visibility of the three-photon lensless ghost image is ∼25%.

To compare the visibility of three-photon lensless ghost imaging with the visibility of two-photon lensless ghost imaging, we turned off the detector D_2 and measured the joint coincidence counts between detectors D_1 and D_3 during scanning. The two-photon lensless ghost image is shown in Fig. 10.

In the figure, the y axis stands for joint coincidence counts collected in 10 s, and the x axis stands for the coordinate of the fiber tip on the detection plane X_2. The circles in the figure stand for the data and the solid line is the fit curve. The single-counting rate of detector D_3 is monitored as constant when fiber tip t_3 is scanning. The visibility of the two-photon lensless ghost imaging is ∼12%. The experimental data in Figs. 9 and 10 show that the visibility of the three-photon lensless ghost imaging is significantly improved compared with that of the two-photon lensless ghost imaging in the photon counting regime.

VI. CONCLUSION

In this article, we report the direct measurement of the third-order temporal and spatial correlation functions of pseudothermal light in the photon-counting regime. The studies show that the probability of jointly detecting three randomly radiated photons from a chaotic thermal source by three individual detectors is 6 times greater if the photodetection events fall in the coherence time and coherence area of the radiation field than if they do not. Phenomenologically, we may name the three-photon correlation "three-photon bunching." From the quantum mechanical point of view, this three-photon bunching is the result of interference between different yet indistinguishable three-photon probability amplitudes. By making use of this property, we measured the three-photon thermal light lensless ghost image and found that the visibility of a ghost image is significantly improved compared with the two-photon ghost image. The studies show that the contrast of thermal light ghost imaging can be improved by higher order detection in the single photon-counting regime.

ACKNOWLEDGMENTS

The authors wish to thank M. H. Rubin, H. Y. Zhang, X. H. He, S. Karmakar, H. Chen, and T. Peng for helpful discussions and suggestions. J.L. would also like to thank G. Q. Zhang. This research was partially supported by the US AFOSR and ARO-MURI program.

[1] T. B. Pittman, Y. H. Shih, D. V. Strekalov, and A. V. Sergienko, Phys. Rev. A **52**, R3429 (1995).
[2] A. Valencia, G. Scarcelli, M. D'Angelo, and Y. H. Shih, Phys. Rev. Lett. **94**, 063601 (2005).
[3] G. Scarcelli, V. Berardi, and Y. H. Shih, Phys. Rev. Lett. **96**, 063602 (2006).
[4] Y. H. Shih, e-print arXiv:0805.1166v5 (2009).
[5] R. S. Bennink, S. J. Bentley, and R. W. Boyd, Phys. Rev. Lett. **89**, 113601 (2002).
[6] A. Gatti, E. Brambilla, M. Bache, and L. A. Lugiato, Phys. Rev. A **70**, 013802 (2004).
[7] M. D'Angelo, Y. H. Kim, S. P. Kulik, and Y. H. Shih, Phys. Rev. Lett. **92**, 233601 (2004).

[8] B. Jack, J. Leach, J. Romero, S. Franke-Arnold, M. Ritsch-Marte, S. M. Barnett, and M. J. Padgett, Phys. Rev. Lett. **103**, 083602 (2009).
[9] I. N. Agafonov, M. V. Chekhova, T. S. Iskhakov, and A. N. Penin, Phys. Rev. A **77**, 053801 (2008).
[10] J. B. Liu and Y. H. Shih, Phys. Rev. A **79**, 023819 (2009).
[11] Y. F. Bai and S. S. Han, Phys. Rev. A **76**, 043828 (2007); D. Z. Cao, J. Xiong, S. H. Zhang, L. F. Lin and K. G. Wang, Appl. Phys. Lett. **92**, 201102 (2008); X. H. Chen, I. N. Agafonov, K. H. Luo, Q. Liu, R. Xian, M. V. Chekhova, and L. A. Wu, e-print arXiv:0902.3713 (2009).
[12] U. Fano, Am. J. Phys. **29**, 539 (1961).
[13] R. Hanbury Brown and R. Q. Twiss, Proc. R. Soc. A **242**, 300 (1957).
[14] D. N. Klyshko, *Photons and Nonlinear Optics* (Gordon and Breach, New York, 1988); L. Mandel and E. Wolf, *Optical Coherence and Quantum Optics* (Cambridge University Press, New York, 1995).
[15] R. J. Glauber, Phys. Rev. **10**, 84 (1963); **130**, 2529 (1963).
[16] M. O. Scully and M. S. Zubairy, *Quantum Optics* (Cambridge University Press, New York, 1997).
[17] M. H. Rubin, Phys. Rev. A **54**, 5349 (1996).
[18] J. Churnside, J. Opt. Soc. Am. **72**, 1464 (1982).
[19] R. Meyers, K. S. Deacon, and Y. H. Shih, Phys. Rev. A **77**, 041801(R) (2008).